Trapping the tetrahedral intermediate in the alkaline phosphatase reaction by substitution of the active site serine with threonine

JIE WANG AND EVAN R. KANTROWITZ

Department of Chemistry, Merkert Chemistry Center, Boston College, Chestnut Hill, Massachusetts 02467, USA

(RECEIVED May 17, 2006; FINAL REVISION July 17, 2006; ACCEPTED July 18, 2006)

Abstract

We report here the construction of a mutant version of *Escherichia coli* alkaline phosphatase (AP) in which the active site Ser was replaced by Thr (S102T), in order to investigate whether the enzyme can utilize Thr as the nucleophile and whether the rates of the critical steps in the mechanism are altered by the substitution. The mutant AP with Thr at position 102 exhibited an ~4000-fold decrease in k_{cat} along with a small decrease in K_m. The decrease in catalytic efficiency of ~2000-fold was a much smaller drop than that observed when Ala or Gly were substituted at position 102. The mechanism by which Thr can substitute for Ser in AP was further investigated by determining the X-ray structure of the S102T enzyme in the presence of the P_i (S102T_P_i), and after soaking the crystals with substrate (S102T_sub). In the S102T_P_i structure, the P_i was coordinated differently with its position shifted by 1.3 Å compared to the structure of the wild-type enzyme in the presence of P_i. In the S102T_sub structure, a covalent Thr-P_i intermediate was observed, instead of the expected bound substrate. The stereochemistry of the phosphorus in the S102T_sub structure was inverted compared to the stereochemistry in the wild-type structure, as would be expected after the first step of a double in-line displacement mechanism. We conclude that the S102T mutation resulted in a shift in the rate-determining step in the mechanism allowing us to trap the covalent intermediate of the reaction in the crystal.

Keywords: X-ray crystallography; mutagenesis; side chain conformation; covalent intermediate; rate-determining step

Escherichia coli alkaline phosphatase (EC 3.1.3.1) is a metalloenzyme that catalyzes the nonspecific hydrolysis of phosphomonoesters to an alcohol and inorganic phosphate (P_i). The enzyme is a dimer of two identical polypeptide chains, each of which contains 449 amino acids and two Zn^{2+} and one Mg^{2+} (Kim and Wyckoff 1989; Stec et al. 2000). The two zinc sites (Zn_1 and Zn_2) are 4 Å apart, and the single magnesium site is located 5 Å from Zn_2 and 7 Å from Zn_1. In the structure of the wild-type noncovalent E·P_i complex (PDB code 1ALK; Kim and Wyckoff 1989), P_i is bound in the active site by interactions with the two zinc atoms and is also positioned in the active site through interactions with the guanidinium nitrogens of Arg166, the backbone nitrogen of Ser102, and a water-mediated interaction with Lys328.

The catalytic mechanism for the alkaline phosphatase reaction was proposed in 1991 and revised in 2000 (Kim and Wyckoff 1991; Stec et al. 2000). The reaction proceeds through a series of four steps: The enzyme binds the

Reprint requests to: Evan R. Kantrowitz, Department of Chemistry, Merkert Chemistry Center, Boston College, Chestnut Hill, MA 02467, USA; e-mail: evan.kantrowitz@bc.edu; fax: (617) 552-2705.

Abbreviations: PNPP, *p*-nitrophenylphosphate; S102T, the mutant version of *E. coli* alkaline phosphatase with Ser102 replaced by Thr; WT_P_i, wild-type *E. coli* alkaline phosphatase with inorganic phosphate bound in the active site (PDB code 1ED8); S102T_P_i, S102T mutant alkaline phosphatase with inorganic phosphate bound in the active site (PDB code 2G9Y); S102T_sub, S102T mutant alkaline phosphatase soaked in PNPP crystal stabilization buffer (PDB code 2GA3).

Article and publication are at http://www.proteinscience.org/cgi/doi/10.1110/ps.062351506.

substrate to form a noncovalent complex (E·ROP); the deprotonated Ser102 hydroxyl group attacks the phosphorus of the substrate to form a covalent serine–phosphate intermediate (E–P_i) (Schwartz and Lipmann 1961; Murphy et al. 1997); a hydroxide ion coordinated to Zn_1 attacks the phosphorus to form a noncovalent enzyme–phosphate complex (E·P_i); and finally, P_i is released, reforming the free enzyme. The rate-determining step of the reaction is pH dependent; at acidic pH, the hydrolysis of the covalent E–P complex is rate-limiting, while under basic conditions the rate-limiting step becomes the dissociation of P_i from the E·P_i noncovalent complex (Hull et al. 1976; Gettins and Coleman 1983).

In a variety of enzymes, Ser and Thr can often be interchanged for many catalytic functions, due to their structural similarity. Some hydrolytic enzymes, such as the asparaginases (Swain et al. 1993; Palm et al. 1996), the proteasome catalytic subunit (Löwe et al. 1995), and aspartyl glucosaminidase (Oinonen et al. 1995), use Thr as a nucleophile instead of Ser. These enzymes have a catalytic mechanism similar to that of the serine proteases, involving the formation of a covalent intermediate. The activation of a Thr nucleophile is different from a Ser nucleophile. Thr is typically activated by a primary amino group from the side chain of Lys or the N-terminal amino acid whereas Ser is activated as part of a catalytic triad.

Although there are no significant chemical differences between the Oγ atoms of Thr and Ser, the side chains of these residues differ substantially in available conformations and size. The side chain of Thr may have an advantage in certain cases, in that the Cγ could help to exclude water from the active site (Dodson and Wlodawer 1998). Gijsbers et al. (2001) have also pointed out the structural and catalytic similarities between alkaline phosphatase and nucleotide pyrophosphatases/phosphodiesterases that utilize a Thr nucleotide in the reaction. Therefore, in this work we construct a mutant version of alkaline phosphatase that has the active site Ser replaced by Thr in order to investigate whether the enzyme can function with a Thr nucleophile. We combine functional characterization of the S102T alkaline phosphatase with two X-ray crystal structures (in the presence P_i and substrate) to understand how Thr functions as a catalytic group in the active site of alkaline phosphatase.

Results and Discussion

Steady-state kinetics of the S102T alkaline phosphatase

The replacement of Ser102 by Thr resulted in a mutant alkaline phosphatase that retained catalytic activity although at reduced levels (Table 1). In the presence of a phosphate acceptor, Tris, the net reaction rate observed is the sum of hydrolysis and transphosphorylation. Under these conditions, the k_{cat} and K_m values for the S102T enzyme decreased 4800-fold and 3.2-fold, respectively, compared to the corresponding values for the wild-type enzyme (Stec et al. 1998), resulting in a 1500-fold decrease in the k_{cat}/K_m ratio. In the absence of a phosphate acceptor, the rate observed is solely hydrolysis. Under these conditions, the k_{cat} and K_m values for the S102T enzyme decreased 3800-fold and 1.7-fold, respectively, compared to the wild-type enzyme (Stec et al. 1998), resulting in a 2200-fold reduction in the k_{cat}/K_m ratio.

Table 1. *Kinetic parameters for the wild-type alkaline phosphatase and the S102T, S102A, S102C, and S102G mutant enzymes at pH 8.0*

Enzyme	k_{cat}[a] (sec^{-1})	K_m (μM)	k_{cat}/K_m (M^{-1} sec^{-1})
In the presence of a phosphate acceptor[b]			
S102G[c]	1.54 (±0.09) × 10^{-3}	145 (±26)	11
S102A[c]	3.03 (±0.05) × 10^{-3}	55 (±4)	55
S102C[c]	104 (±8) × 10^{-3}	541 (±79)	192
S102T	16.6 (±1.5) × 10^{-3}	6.56 (±1.64)	2530
WT[c]	79.8	21	3.8 × 10^6
In the absence of a phosphate acceptor[d]			
S102G[c]	1.18 (±0.03) × 10^{-3}	195 (±11)	12
S102A[c]	1.34 (±0.06) × 10^{-3}	44 (±8)	30
S102C[c]	176 (±5) × 10^{-3}	267 (±19)	659
S102T	11.8 (±0.0) × 10^{-3}	5.79 (±0.0)	2030
WT[c]	44.8	10	4.5 × 10^6

[a] The k_{cat} values were calculated from the V_{max} value obtained by using a dimer molecular mass of 94,000 Da.
[b] Assays were performed at 25°C in 1.0 M Tris buffer (pH 8.0) with PNPP as substrate.
[c] Data from Stec et al. (1998).
[d] Assays were performed in 0.010 M Tris with the ionic strength adjusted with NaCl to equal 1.0 M Tris.

Although the S102T enzyme is much less active than the wild-type enzyme, it is far more active than the previously reported S102C, S102A, and S102G enzymes, either in the presence or in the absence of a phosphate acceptor (Stec et al. 1998). In the presence of a phosphate acceptor, the k_{cat}/K_m ratio of the S102T enzyme was 230-fold, 46-fold, and 13-fold higher than the corresponding values for the S102G, S102A, and S102C enzymes, respectively. In the absence of a phosphate acceptor, the k_{cat}/K_m ratio was 169-fold, 68-fold, and 3.1-fold higher. When the data for the S102T enzyme reported here are combined with data for other mutations at position 102 (Stec et al. 1998), the catalytic activity of these enzymes in decreasing activity is found to be WT > S102T > S102C > S102A > S102G.

Structure of the S102T_P_i enzyme

The structure of the S102T in the presence of P_i was determined in order to elucidate the structure of the noncovalent E·P_i complex. Crystals of the S102T enzyme

were soaked in a phosphate-containing buffer for 15 min before data collection. Analysis of $2F_o$–F_c and F_o–F_c electron density maps indicated that the active sites in the S102T_P_i structure differed significantly from the corresponding wild-type structure (WT_P_i), particularly near the phosphate binding sites. The active site of the S102T_P_i structure is shown in Figure 1A. The side chain methyl group of Thr102 restricts the available conformations of the Thr side chain, so that the hydroxyl group cannot rotate as freely as was observed for the Ser hydroxyl group. The orientations of the Thr side chain are limited to three χ values: −60°, +180°, and +60° (Daley and Sykes 2003). In the S102T_P_i structure, the side chain of Thr102 adopts different conformations in the A-chain and B-chain. In the A-chain, the side chain of the Thr102 adopts the $\chi = -60°$ conformation, while in the B chain it adopts the $\chi = +180°$ conformation. In chain A, the methyl group of Thr102 points toward the midpoint of the two hydrogen bonds that form between a phosphorus oxygen and the side chain of the Arg166 in the WT_P_i structure (see Fig. 1C). If one compares the position of Thr102 in the S102T_P_i structure with the position of P_i and Arg166 in the WT_P_i structure, the distance between the methyl group and the phosphorus oxygen is 2.2 Å, while the distance between the methyl group and the Arg166 NH1 is 2.8 Å. This close contact between a hydrophobic group and two hydrophilic groups is energetically unfavorable, resulting in the displacement of P_i by 1.3 Å in the S102T_P_i structure, compared to its position in the WT_P_i structure. The new position prevents the P_i from forming two hydrogen bonds with Arg166, important interactions for the stabilization of P_i in the active site (Chaidaroglou et al. 1988; Chen et al. 1992). In addition, in the S102T_P_i structure, the P_i is stabilized by two coordinate bonds with Zn_1, but has one fewer coordinate bond with Zn_2.

In chain B of the S102T_P_i structure, the hydroxyl group of Thr102 forms a direct coordinate bond with Zn_2, preventing the P_i from making a coordinate bond with Zn_2 (see Fig. 1D). P_i makes two coordinate bonds with Zn_1, but does not interact with Arg166, exhibiting displacement of 1.1 Å compared to its position in the WT_P_i structure.

The S102T_sub structure—Trapping the covalent E–P_i intermediate

In an attempt to determine the structure of the alkaline phosphatase E·S complex, the X-ray structure of the S102T enzyme was determined using crystals of the S102T enzyme that were frozen after being soaked for a short time in buffer containing the substrate, *p*-nitrophenol phosphate. The 2.2 Å S102T_sub structure was refined to a R_{factor}/R_{free} of 0.192/0.229 in the I222 space group. In the active site of this structure, the $2F_o$–F_c and F_o–F_c electron density maps showed continuous density between the phosphorus and the Oγ of the Thr102, with a P–O bond distance of 1.6 Å in both the A and B chains (see Fig. 1B,E). The average distance of a P–O covalent bond is 1.7 Å. These two observations indicate that the structure was not of the E·S complex, but rather of the covalent E–P_i complex. To confirm this hypothesis, a phosphothreonyl residue (ThP102) was modeled into the active sites of both the A and B chains. The S102T_sub structure was then further refined with Thr102 replaced by ThP102. In the S102T_sub structure the active sites of the A and B chains are virtually identical. The average B factor for the side chain of ThP102 was 34.7 $Å^2$, close to the average B factor for the side chains of the entire protein, 32.3 $Å^2$ (Table 2). In the refined structure, one of the phosphate oxygens of ThP102 was coordinated to Zn_1 while another oxygen was coordinated to Zn_2. The stereochemistry of the phosphorus in the S102T_sub structure is inverted compared to the stereochemistry of the P_i in the structure of the wild-type noncovalent E·P_i structure, as would be expected after the first step of a double in-line displacement mechanism (see Fig. 1F).

The rate of hydrolysis of the covalent E–P_i complex is greatly reduced

In the proposed mechanism for reaction of native alkaline phosphatase, a water molecule activated by Zn_1 acts as the nucleophile in the second in-line displacement step: the hydrolysis of the covalent E–P complex to form the E·P_i noncovalent complex. In a previously determined structure of an alkaline phosphatase mutant in which histidine 331 was replaced by glutamine, the covalent Ser–P_i complex was stabilized (Murphy et al. 1997). In this structure, a water molecule was observed coordinated to Zn_1, positioned optimally for in-line displacement of the P_i. However, in the S102T_sub structure, no water molecule was observed in the same position in either the A- or B-chain active sites. The methyl group of the ThP102 points toward the hydroxyl group of Thr155. Because of the repulsion force between a hydrophobic and hydrophilic group, the hydroxyl of Thr155 in the threonine–phosphate complex is displaced away from the active site, when compared to the covalent serine–phosphate complex (PDB code 1HJK; Murphy et al. 1997). The hydroxyl group of Thr155 is shifted 1.2 Å and 0.7 Å away from the active site in the A and B chains, respectively. This movement changes the active site geometry and may be the reason for the weaker binding of the nucleophilic water molecule, which in turn, results in the reduced rate of hydrolysis observed for the S102T enzyme as compared to the wild-type enzyme.

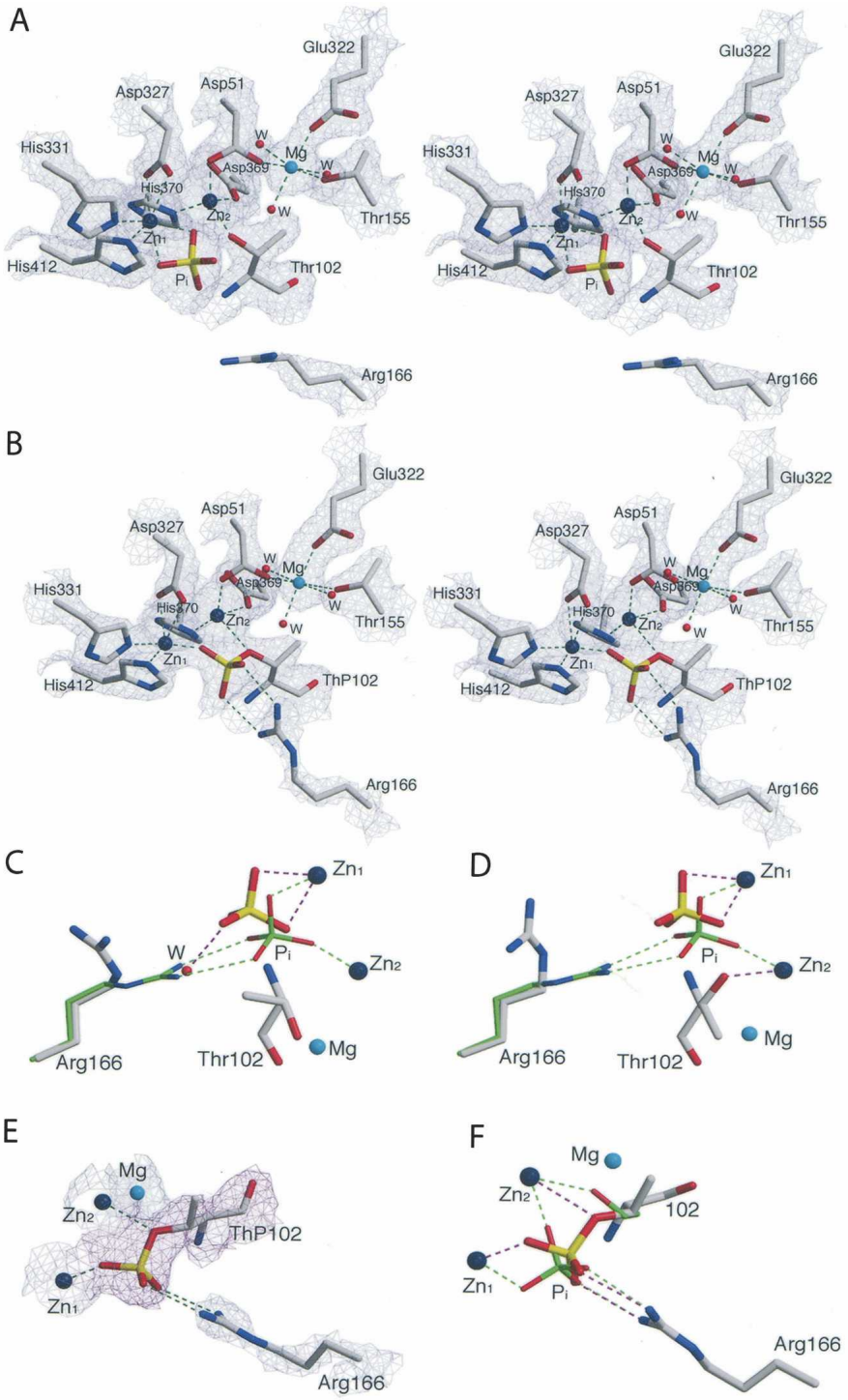

Figure 1. (*A*) Stereoview of the active site of the S102T_P_i structure. Shown is the $2F_o$–F_c electron density map for the A chain (1.2 σ). The side chain of the Thr102 are in the $\chi = -60°$ conformation). Water molecules are shown as red spheres and zinc and magnesium atoms as large dark blue and cyan spheres. Dashed lines represent hydrogen bonds. (*B*) Stereoview of the $2F_o$–F_c electron density map for the B chain of S102T_sub (1.2 σ). (*C*) Comparison of Arg166 and P_i in the active sites of the S102T_P_i structure (elemental colors, thick lines) and the WT_P_i structure (PDB code 1ED8; Stec et al. 2000; green, thin) in the A chain and in the B chain (*D*). Ligands around the metals are not shown. (*E*) Active site of the S102T_sub structure. The Arg166 and metals are overlaid on the $2F_o$–F_c electron density map (blue) shown contoured at 1.2 σ. The ThP102 is overlaid on the F_o–F_c electron density map (magenta) shown contoured at 1.5 σ. (*F*) Comparison of P_i and Ser102 (ThP102) in the active site of the S102T_sub structure (elemental colors, thick lines) and the WT_P_i (green, thin) structure. Ligands around the metals are not shown. Figures were prepared using MOLSCRIPT (Kraulis 1991).

Table 2. *Summary of the B factors of the side chains*

	B factor (Å^2)		
	WT_P_i[a]	S102T_sub[a]	S102T_P_i[a]
Protein	25	32	28
Arg166			
A chain	14	29	42
B chain	22	32	48
Thr102 (ThP102)			
A chain	—	33	30
B Chain	—	37	29
P_i[b]			
A chain	19	35	44
B chain	23	39	47

[a] WT_P_i, wild-type *E. coli* alkaline phosphatase with inorganic phosphate bound in the active site (PDB code 1ED8); S102T_P_i, S102T mutant alkaline phosphatase with inorganic phosphate bound in the active site (PDB code 2G9Y); S102T_sub, S102T mutant alkaline phosphatase soaked in PNPP crystal stabilization buffer (PDB code 2GA3).
[b] The P_i in the S102T_sub refers to the phosphate moiety in ThP102 residue.

Arg166 is involved in transition state stabilization and the release of the P_i

Previous studies have suggested that Arg166 has two functions in the catalytic mechanism. First, it assists in substrate binding and the release of P_i and second, it stabilizes the charge on the covalent E–P intermediate and the trigonal bipyramidal transition state during the reaction (Chaidaroglou et al. 1988; Kim and Wyckoff 1991). Arg166 was observed to occupy different positions in the S102T_sub and S102T_P_i structures. In both chains of the S102T_sub structure, the guanidinium group of the Arg166 interacts with the phosphate moiety of ThP102 (see Fig. 1F), helping to stabilize the covalent E–P_i intermediate. In contrast, in both chains of the S102T_P_i structure, Arg166 rotates to a new position away from the P_i binding pocket. In this conformation Arg166 forms two fewer hydrogen bonds with P_i than are observed in the WT_P_i structure (see Fig. 1C,D). The loss of these interactions results in a dramatic increase in the average B factor of the Arg166 side chain to 44.9 Å^2, an ~60% increase compared to the average B factors of the protein (Table 2). This significant increase in the average B factor of Arg166 side chain suggests that this side chain has considerably more flexibility in the S102T_P_i structure. In this structure, a water molecule interacts with P_i in the position normally occupied by Arg166 in the WT_P_i structure. However, the electron density for this water is weak (1.2 σ), and there is no water at the equivalent position in chain B. With the loss of the interactions between P_i and Arg166, the B factors for the P_i are dramatically increased compared to the values observed for P_i in the wild-type structure (WT_P_i) (Table 2).

Previous studies of a mutant alkaline phosphatase in which Asp101 was converted to Ser have shown that increased flexibility of the Arg166 side chain correlates with a faster dissociation of P_i and a high rate of catalysis (Chen et al. 1992). For the wild-type enzyme, Arg166 is positioned rigidly in a hydrogen bonding network that includes two hydrogen bonds with P_i, one with Asp101 and two with a water molecule (Kim and Wyckoff 1991; Stec et al. 2000). However, in the S102T_P_i structure, there is a repulsion between the methyl group of Thr102 and P_i, resulting in the inability of P_i to bind in the same position observed in the wild-type enzyme. The P_i shifts position until it is restabilized by Zn_2. This positional shift of the P_i breaks the hydrogen bonding network of the active site, especially the part involving Arg166. Without these interactions, Arg166 becomes unstable in the position observed in the WT_P_i structure and therefore moves to a more stable position. Both the side chain of Arg166 and P_i have enhanced mobility in this structure, which results in a weakening of affinity for P_i and a faster release of the P_i from the noncovalent E·P_i complex.

Conclusions

Our ability to trap the covalent E–P_i intermediate in the S102T_sub structure indicates that the rate-determining step in the mechanism has changed for the S102T enzyme. In the case of the S102T enzyme, hydrolysis of the covalent E–P_i intermediate now becomes slow relative to release of P_i from the noncovalent E·P_i complex. Thus, in the S102T enzyme the chemical step of hydrolysis of the E–P_i complex becomes rate limiting, thereby allowing us to trap the covalent intermediate in the crystal.

The crystal structures of the S102T_sub and S102T_P_i enzymes suggest the manner in which the rate-determining step in the mechanism was changed by the mutation of Ser102 to Thr. The methyl group of Thr102 induces changes in the positions of active site residues, resulting in a weaker binding of the water molecule that acts as the nucleophile in the second step in the mechanism. This reduced availability of the entering nucleophile results in a significant decrease in the rate of the hydrolysis of the E–P covalent complex. Since the release of P_i is the rate-determining step for wild-type enzyme at alkaline pH, a slower hydrolysis rate of the E–P complex results in a shift in the rate-determining step from the dissociation of P_i from the E·P_i noncovalent complex to the hydrolysis of E–P covalent complex in the S102T enzyme. The reduced affinity of the catalytic water explains the ~2000-fold decrease of the enzyme activity of the S102T enzyme as compared to the wild-type enzyme.

This S102T mutation in alkaline phosphatase has consequences that are similar to the Glu to Asp mutation in the active sites of triosephosphate isomerases. In both cases while the overall chemical mechanism is retained, the mutation changes the relative free energy of the

transition states of the individual steps and results in a different rate-determining step (Raines et al. 1986).

Materials and methods

Materials

Ampicillin, magnesium chloride, zinc chloride, sodium chloride, sodium dihydrogen phosphate, EDTA, sucrose, sodium dodecyl sulfate, and *p*-nitrophenyl phosphate were purchased from Sigma Chemical Co. Tris and enzyme grade ammonium sulfate were purchased from ICN Biomedicals. Tryptone and yeast extract were obtained from Difco Laboratories. The oligonucleotides required for site-specific mutagenesis and sequencing were obtained from Operon Technologies. The QuikChange Mutagenesis kit was supplied by Stratagene. Kits for plasmid isolation and purification were supplied by Qiagen. DNA grade agarose was from Fisher. Protein Assay Dye and Source 15Q strong anion-exchange resin were obtained from Bio-Rad. Crystal cryo-mounting loops were from Hampton Research.

Construction of the S102T alkaline phosphatase by site-specific mutagenesis

The S102T mutation was introduced in the *phoA* gene using the procedure outlined by Stratagene in the QuikChange Mutagenesis kit protocol. The entire gene was sequenced to ensure that no other mutations had been introduced during the mutagenesis. The final plasmid containing the S102T mutation in the *phoA* gene was designated pEK625.

Expression of the S102T alkaline phosphatase

E. coli SM547 [Δ(*phoA-phoC*), *phoR*, tsx::Tn5, Δ*lac*, *galK*, *galU*, *leu*, str^r] was used as the host strain for the expression of the S102T alkaline phosphatase. Since the chromosomal *phoA* gene was deleted from the strain, all the alkaline phosphatase produced is expressed from the *phoA* gene on the plasmid. The mutation in the *phoR* regulatory gene results in constitutive synthesis of alkaline phosphatase.

Purification of the S102T alkaline phosphatase

The S102T enzyme was isolated from the SM547/pEK625 plasmid/strain combination by the method previously described (Chaidaroglou et al. 1988). The purity of the enzyme was checked by SDS-polyacrylamide gel electrophoresis (Laemmli 1970). The Bio-Rad version of Bradford's dye-binding assay was used to determine protein concentrations using the wild-type alkaline phosphatase as the standard (Bradford 1976).

Determination of enzymatic activity

Phosphatase activity was measured spectrophotometrically at 25°C utilizing *p*-nitrophenyl phosphate as substrate by monitoring the release of *p*-nitrophenylate at 410 nm (Garen and Levinthal 1960). The sum of the hydrolase and transferase activities was determined using 1.0 M Tris as the phosphate acceptor. The hydrolase activity was measured using 0.010 M Tris as the buffer. The ionic strength of the two Tris buffers was maintained constant using NaCl.

Crystallization

The vapor diffusion method was used to crystallize the enzyme using hanging drops of 2 μL. The enzyme solution was dialyzed against a protein-stabilization buffer of 100 mM Tris (pH 9.5), 10 mM $MgCl_2$, 0.01 mM $ZnCl_2$, and 0.85 M $(NH_4)_2SO_4$ before being concentrated to ~40 mg/mL. Within ~1 mo, crystals formed in the drops with ammonium sulfate concentrations between 2.0 M and 2.2 M. Crystal sizes varied from $0.2 \times 0.2 \times 0.1$ mm^3 to $1.2 \times 0.6 \times 0.3$ mm^3.

Crystal mounting and data collection

Crystals were initially transferred into a crystal stabilization buffer composed of 3.0 M $(NH_4)_2SO_4$, 100 mM Tris (pH 7.5), 10 mM $MgCl_2$, and 2 mM $ZnCl_2$ for at least 24 h. A $0.3 \times 0.25 \times 0.2$ mm^3 crystal was soaked in a *p*-nitrophenylphosphate (PNPP) crystal stabilization buffer (10 mM PNPP, 3.0 M $(NH_4)_2SO_4$, 100 mM Tris, 10 mM $MgCl_2$, 2 mM $ZnCl_2$ at pH 7.5) for 15 min before it was soaked into a mixture containing 80% *p*-nitrophenyl phosphate crystal stabilization buffer and 20% glycerol for 1 min (S102T_sub crystal). Another $0.2 \times 0.1 \times 0.1$ mm^3 crystal was first soaked in a P_i crystal stabilization buffer (2 mM NaH_2PO_4, 3.0 M $(NH_4)_2SO_4$, 100 mM Tris, 10 mM $MgCl_2$, 2 mM $ZnCl_2$ at pH 7.5) for 15 min before it was soaked into a mixture of 80% P_i crystal stabilization buffer and 20% glycerol for 1 min (S102T_P_i crystal). Crystals were picked up in cryo-loops and frozen in liquid nitrogen.

The diffraction data were collected at the Crystallographic Facility in the Chemistry Department of Boston College, using a Rigaku RU-200 rotating anode generator, operating at 50 kV and 100 mA, equipped with a Rigaku/MSC R-axis IV++ detector. Diffraction data were collected to 2.20 Å and 2.00 Å, respectively, for the S102T_sub and S102T_P_i crystals (Table 3). The data sets were integrated, scaled, and averaged by using d*TREK (Rigaku/MSC) (Pflugrath 1999).

Structure refinement

The initial models for both the S102T_sub and the S102T_P_i structures were the coordinates of wild-type *E. coli* alkaline phosphatase with Co^{2+} in all the metal sites determined to 1.60 Å (PDB code 1Y6V; Wang et al. 2005). This initial coordinate was chosen because the S102T structures are in the same space group I222 and have almost identical unit cell dimensions. Before refinement, all ligands and waters were removed from the model and the Ser102 residue was replaced by Thr in XtalView (McRee 1999). Refinements were carried out using the Crystallography & NMR System (CNS) (Brunger et al. 1998). After the first rigid body refinement, simulated annealing (Brunger et al. 1997), energy minimization, and B-factor refinement, initial maps were inspected and manual rebuilding was performed in XtalView. After each round of refinement, R_{free} was used to avoid overfitting and the F_o–F_c electron density map was visually inspected for alternate positions (Kleywegt and Brunger 1996). When the R_{factor} fell below 25%, waters were added on the basis of peaks in the F_o–F_c electron density maps that were at or above the 3σ level, and were checked and retained only when they could be justified by hydrogen bonding interactions. With approximately 520 and 560 waters, the S102T_sub and the S102_P_i structures were refined to an R_{factor}/R_{free} of 19.2%/22.9% and 20.5%/24.2% at a resolution of 2.20 Å and 2.00 Å, respectively (see Table 3).

Table 3. *Data collection and refinement summary of the S102T_sub and S102T_P_i structures*

	S102T_sub	S102T_P_i
Data collection		
Space group	I222	I222
Resolution (Å)[a]	14.98–2.20 (2.28–2.20)	32.70–2.00 (2.07–2.00)
Total reflections	193,898	290,840
Unique reflections	55,816	81,469
Redundancy[a]	3.47 (3.33)	3.57 (3.49)
Completeness (%)[a]	90.3 (92.6)	99.2 (97.8)
Unit cell (Å)	$a = 76.23$	$a = 76.46$
	$b = 164.97$	$b = 164.49$
	$c = 192.90$	$c = 192.53$
Angles	$\alpha = \beta = \gamma = 90°$	(same)
R_{merge} (%)[a,b]	7.7 (35.2)	8.6 (34.6)
Refinement		
Resolution (Å)	14.98–2.20	32.70–2.00
Average (I/σ)	11.3	9.2
R_{factor}	0.192	0.205
R_{free}	0.229	0.242
Waters	518	559
Statistics (RMS deviations)		
Bonds (Å)	0.005	0.005
Angles (°)	1.33	1.35
Impropers (°)	0.804	0.794
Dihedrals (°)	23.21	23.04

[a] Data in parentheses correspond to highest resolution shell.
[b] $R_{merge} = \sum (I_{hkl} - I_{\bar{h}\bar{k}\bar{l}}) / \sum I_{\bar{h}\bar{k}\bar{l}}$, where I_{hkl} is the observed intensity and $I_{\bar{h}\bar{k}\bar{l}}$ is the mean intensity of the observed intensity.

Stereochemical quality of the two structures was determined from the Ramachandran plot using PROCHECK (Laskowski et al. 1993). Both structures have more than 90% of the residues within the most favored region. None of the active site residues were in disallowed regions. The details of data processing and refinement statistics for both structures are reported in Table 3. The atomic coordinates of the S102T_P_i and S102T_sub structures have been deposited in the Protein Data Bank as entries 2G9Y and 2GA3, respectively.

Acknowledgments

This work was partially supported by Grant GM42833 from the National Institutes of Health.

References

Bradford, M.M. 1976. A rapid and sensitive method for the quantitation of microgram quantities of protein utilizing the principle of protein-dye binding. *Anal. Biochem.* **72:** 248–254.

Brunger, A.T., Adams, P.D., and Rice, L.M. 1997. New applications of simulated annealing in X-ray crystallography and solution NMR. *Structure* **5:** 325–336.

Brunger, A.T., Adams, P.D., Clore, G.M., DeLano, W.L., Gros, P., Grosse-Kunstleve, R.W., Jiang, J.S., Kuszewski, J., Nilges, M., and Pannu, N.S.1998. Crystallography & NMR system: A new software suite for macromolecular structure determination. *Acta Crystallogr. D Biol. Crystallogr.* **54:** 905–921.

Chaidaroglou, A., Brezinski, J.D., Middleton, S.A., and Kantrowitz, E.R. 1988. Function of arginine in the active site of *Escherichia coli* alkaline phosphatase. *Biochemistry* **27:** 8338–8343.

Chen, L., Neidhart, D., Kohlbrenner, W.M., Mandecki, W., Bell, S., Sowadski, J., and Abad-Zapatero, C. 1992. 3-D structure of a mutant (Asp101 → Ser) of *E. coli* alkaline phosphatase with higher catalytic activity. *Protein Eng.* **5:** 605–610.

Daley, M.E. and Sykes, B.D. 2003. The role of side chain conformational flexibility in surface recognition by *Tenebrio molitor* antifreeze protein. *Protein Sci.* **12:** 1323–1331.

Dodson, G. and Wlodawer, A. 1998. Catalytic triads and their relatives. *Trends Biochem. Sci.* **23:** 347–352.

Garen, A. and Levinthal, C. 1960. A fine-structure genetic and chemical study of the enzyme alkaline phosphatase of *E. coli*. 1. Purification and characterization of alkaline phosphatase. *Biochim. Biophys. Acta* **38:** 470–483.

Gettins, P. and Coleman, J.E. 1983. ^{31}P nuclear magnetic resonance of phosphoenzyme intermediates of alkaline phosphatase. *J. Biol. Chem.* **258:** 408–416.

Gijsbers, R., Ceulemans, H., Stalmans, W., and Bollen, M. 2001. Structural and catalytic similarities between nucleotide pyrophosphatases/phosphodiesterases and alkaline phosphatases. *J. Biol. Chem.* **276:** 1361–1368.

Hull, W.E., Halford, S.E., Gutfreund, H., and Sykes, B.D. 1976. ^{31}P nuclear magnetic resonance study of alkaline phosphatase: The role of inorganic phosphate in limiting the enzyme turnover rate at alkaline pH. *Biochemistry* **15:** 1547–1561.

Kim, E.E. and Wyckoff, H.W. 1989. Structure of alkaline phosphatase. *Clin. Chim. Acta* **186:** 175–188.

———. 1991. Reaction mechanism of alkaline phosphatase based on crystal structures: Two-metal ion catalysis. *J. Mol. Biol.* **218:** 449–464.

Kleywegt, G.J. and Brunger, A.T. 1996. Checking your imagination: Application of the free *R* value. *Structure* **4:** 897–904.

Kraulis, P.J. 1991. MOLSCRIPT: A program to produce both detailed and schematic plots of protein structures. *J. Appl. Crystallogr.* **24:** 946–950.

Laemmli, U.K. 1970. Cleavage of structural proteins during the assembly of the head of bacteriophage T4. *Nature* **227:** 680–685.

Laskowski, R.A., MacArthur, M.W., Moss, D.S., and Thornton, J.M. 1993. PROCHECK: A program to check the stereochemical quality of protein structures. *J. Appl. Crystallogr.* **26:** 283–291.

Löwe, J., Stock, D., Jap, B., Zwickl, P., Baumeister, W., and Huber, R. 1995. Crystal structure of the 20S proteasome from the Archaeon *T. acidophilum* at 3.4 Å resolution. *Science* **268:** 533–539.

McRee, D.E. 1999. XtalView/Xfit—A versatile program for manipulating atomic coordinates and electron density. *J. Struct. Biol.* **125:** 156–165.

Murphy, J.E., Stec, B., Ma, L., and Kantrowitz, E.R. 1997. Trapping and visualization of a covalent enzyme–phosphate intermediate. *Nat. Struct. Biol.* **4:** 618–621.

Oinonen, C., Tikkanen, R., Rouvinen, J., and Peltonen, L. 1995. Three-dimensional structure of human lysosomal aspartylglucosaminidase. *Nat. Struct. Biol.* **2:** 1102–1108.

Palm, G.J., Lubkowski, J., Derst, C., Schleper, S., Rohm, K.H., and Wlodawer, A. 1996. A covalently bound catalytic intermediate in *Escherichia coli* asparaginase: Crystal structure of a Thr-89-Val mutant. *FEBS Lett.* **390:** 211–216.

Pflugrath, J.W. 1999. The finer things in X-ray diffraction data collection. *Acta Crystallogr. D Biol. Crystallogr.* **55:** 1718–1725.

Raines, R.T., Sutton, E.L., Straus, D.R., Gilbert, W., and Knowles, J.R. 1986. Reaction energetics of a mutant triosephosphate isomerase in which the active-site glutamate has been changed to aspartate. *Biochemistry* **25:** 7142–7154.

Schwartz, J.H. and Lipmann, F. 1961. Phosphate incorporation into alkaline phosphatase of E. coli. *Proc. Natl. Acad. Sci.* **47:** 1996–2005.

Stec, B., Hehir, M.J., Brennan, C., Nolte, M., and Kantrowitz, E.R. 1998. Kinetic and X-ray structural studies of three mutant *E. coli* alkaline phosphatases: Insights into the catalytic mechanism without the nucleophile Ser-102. *J. Mol. Biol.* **277:** 647–662.

Stec, B., Holtz, K.M., and Kantrowitz, E.R. 2000. A revised mechanism of the alkaline phosphatase reaction involving three metal ions. *J. Mol. Biol.* **299:** 1303–1311.

Swain, A.L., Jaskolski, M., Housset, D., Rao, J.K.M., and Wlodawer, A. 1993. Crystal structure of *Escherichia coli* L-asparaginase, an enzyme used in cancer therapy. *Proc. Natl. Acad. Sci.* **90:** 1474–1478.

Wang, J., Stieglitz, K.A., and Kantrowitz, E.R. 2005. Metal specificity is correlated with two crucial active site residues in *Escherichia coli* alkaline phosphatase. *Biochemistry* **44:** 8378–8386.